Electrostatic Model of Metal-Induced Gap States in Metal Edge, Top and Hybrid Contacts to MoS2 transistors

E. Deylgat[1,2,3], C.P. Chuu[4], E. Chen[4], B. Sorée[2,3,5] and W. Vandenberghe[1]
[1]Univerty of Texas at Dallas, Dallas, TX, USA, [2]Catholic University of Leuven, Leuven, BE, [3]IMEC, Leuven, BE,[4]Corporate Research, Taiwan Semiconductor Manufacturing Company Ltd., Hsinchu, Taiwan, [5]University of Antwerp, Antwerp, BE

Introduction: Two-dimensional (2D) semiconducting materials are a potential replacement for silicon-based channels in future transistor designs. Transition-metal dichalcogenides (TMDs) such as MoS_2, WS_2, and WSe_2 are some of the most promising candidates due to their relatively high band gaps and decent mobilities [1]. However, a key challenge of using 2D materials is the high contact resistance between the metal/TMD interface which is often characterized by so-called Schottky barriers. In the past, Schottky barriers were described by the Schottky-Mott rule in which the barrier height (BH) depends on the contact metal work function (WF). However, in many cases, the barrier is rather insensitive to the metal WF as the Fermi level (FL) is "pinned" to a certain energy level [2]. The pinning often occurs due to MIGS, due to which the FL is pinned to the charge neutrality level ECNL resulting in increased contact resistance.

In this paper, we model the MIGS in metal contacts with different geometries, the edge, top and hybrid contact (EC, TC and HC). From the model, we extract MIGS densities corresponding to different pinning parameters and compare to DFT and experiments. We calculate the contact resistance for back-gated contacts and determine current paths of different contact geometries.

Methods: Figure 1 shows a schematic of the EC, TC, and HC (top to bottom) and defines the 2D material thickness t_{2D} = 0.65 nm, the contact length L_C = 6 nm, the van-der-Waals (vdW) gap thickness as t_{vdW} = 0.3 nm and the back-gate distance as L_{BG} = 100 nm.

Figure 2 shows a schematic of the FL pinning mechanism due to MIGS described by Eq. (4, 5).

Figure 6 shows a schematic of the HC geometry where we indicate the location of the top and edge MIGS in the Poisson model.

Figure 3 shows a flowchart of the methodology of the BH model and transport calculation. We numerically solve the Poisson equation (Eq. (1)), self-consistently with the electron concentration in a 2D material (Eq. (2)) using finite element code [3]. We determine the IFBL by using an analytical expression (Eq. (3)) [4] which is added to the solution of the Poisson equation. To determine the FL pinning, we measure the BH in the center of the TMD and fit the S-parameter (Eq. (5)). We calculate the contact resistance by setting up an effective mass Hamiltonian (Eq. (6)) which is discretized with the finite-differences method. We use the quantum boundary transmission method (Eq. (7, 8)) [5, 6] to extract the transmission which is used in Eq. (9) to arrive at the contact resistance.

Results: Figure 4(a) shows the potential energy U of the EC, TC, and HC from top to bottom. The top dielectric is air, while the bottom dielectric is SiO_2. Figure 4(b) shows the solution of the Poisson equation (Eq. (1)) for the different geometries. Figure 4(c) shows the IFLB where we assume a homogeneous dielectric of SiO_2.

Figures 5(a) and (b) show the Schottky barrier height as a function of the difference between the metal WF and the MoS_2 electron affinity for contacts with different geometries and substrates. In the case of the EC (Fig. 5(a)), very high MIGS densities are needed to pin significantly. At a very high density of D_{IT} = 1e15 cm^{-2} eV^{-1}, we realize S = 0.67. Compare that to the pinning in the TC case (Fig. 7(b)), we see that full pinning is achieved at $D_{IT} > 10^{15}$ cm^{-2} eV^{-1} as S = 0.02 while very low pinning is achieved at $D_{IT} < 1\times10^{11}$ cm^{-2} eV^{-1} (S = 0.97). Previously, the BH was determined experimentally for Ti, Ni, and Pt in both EC and TC on SiO_2 substrates in ref. [7]. Pinning-free ECs were fabricated, and the extracted barrier heights are indicated in Fig. 5a. The corresponding S-parameter is S > 0.88 which translates to $D_{IT} <$ 1e14 cm^{-2} eV^{-1}. Pinning-free ECs can be fabricated if the interfaces are defect-free as the MIGS do not contribute much to pinning. In the case of the TC (Fig. 5(b)), the barriers from ref. [4] correspond to a $D_{IT} = 1.3\times10^{14}$ cm^{-2} eV^{-1}. Following Eq (3), we determine MIGS = 2.6×10^{13} cm^{-2}.

Figures 7(a) and (b) show the contact resistance as a function of carrier concentration for the different contact geometries in the case of a (a) Ni and (b) an Sb contact. The corresponding spatial current densities at the highest carrier densities are shown in Fig. (c) and (d), respectively. For the Sb contact, the contact resistance is close to the quantum limit (QL), since the barrier is low and MIGS are assumed to be low due to Sb being a semi-metal. The HC yields the lowest resistance since more current paths are available. The top contact has higher resistance because the current must tunnel through the vdW gap. For the Ni contact, the barrier is high. Therefore, the resistance is the lowest in the TC since the EC yields higher barriers in the x-direction. Most of the current goes through the metal corner of the hybrid and TCs. However, the HC has high resistance since the vicinity of the edge metal boundary increases the barrier.

Figure 8(a) shows the DFT structure of a top-contacted MoS_2 monolayer with a metal (Au). Figure 8 (b) shows the density of states (DOS) of the MoS_2 monolayer. The MIGS = 1.2×10^{13} cm^{-2} are extracted from DOS inside the bandgap of the monolayer induced by the metal. Figure 8(c) shows the DFT structure of an edge geometry. Figure 8(d) shows the MIGS as a function of x-coordinate along the length of the monolayer. At the edges, we find MIGS = 2.3×10^{13} cm^{-2}. The MIGS obtained from DFT is of the same order as the MIGS from the model fitted to the experimental data. Table 1 shows the values of the MIGS and E_{CNL} in the case of the EC and TC using the Poisson equation and the DFT.

Conclusion: We modeled the MIGS in EC, TC, and HC. MIGS pin the FL at much lower concentrations in TCs compared to ECs, allowing for easier pinning free edge contacts. However, EC do not yield the best performance. In low barrier scenarios, the HC gets closest to the QL, while the the TC yields the lowest contact resistance in high barrier scenarios.

References: [1] Y. Liu, *et al*. *Nature* **591**, 43–53 (2021). [2] A. Allain, *et al*. *Nat. Mat.* **14**, 1195–1205 (2015). [3] A. Logg, et al. ACM Trans. Math. Soft. **37** (2010). [4] S. R. Evans, *et al. Phys. Rev. Appl.* **20**, 044003 (2023). [5] M. Fischetti and W. Vandenberghe (2016). [6] C. S. Lent, et. al, JAP **67**, 6353–6359 (1990). [7] T. Y. T. Hung, *et al. IEDM* (2020).

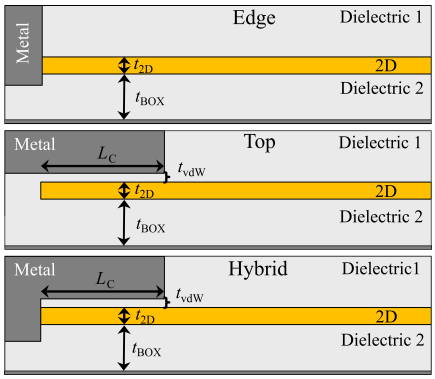

Fig. 1. Contact geometries considered in simulations.

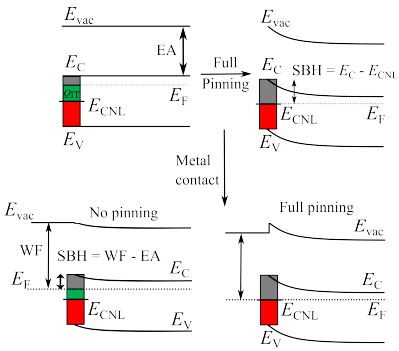

Fig. 2. Schematic Fermi level pinning of MoS_2 bands in the presence of MIGS.

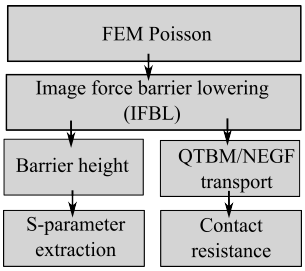

Fig. 3. Flow chart of the methodology of obtaining the barrier height for S-parameter extraction or obtaining contact

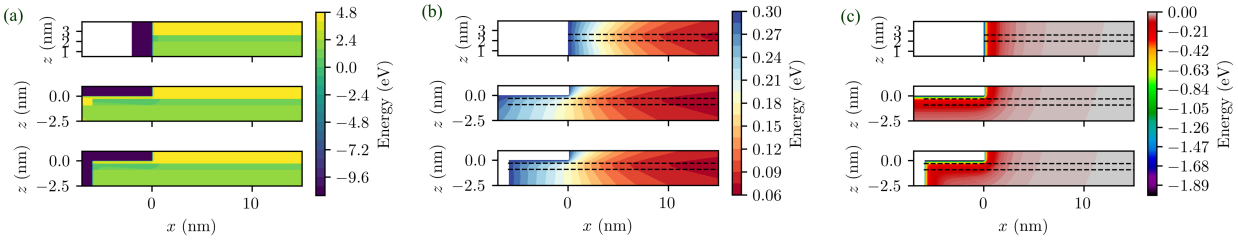

Fig. 4. (a) Energy landscape of the edge, top and hybrid contact (top to bottom). (b) Solution of Poisson equation for edge, top and hybrid contact (without MIGS). (c) Image-force barrier-lowering potential energy for edge, top and hybrid contact.

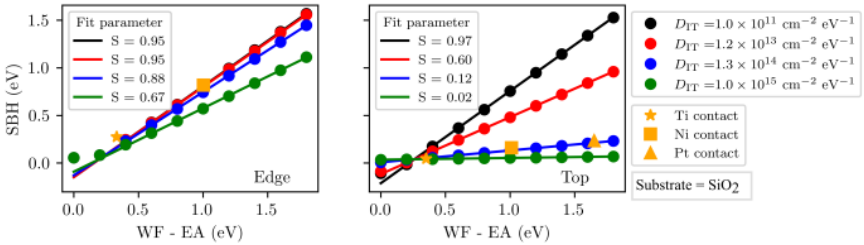

Fig. 5. Schottky barrier height vs. difference metal WF and MoS_2 EA for different MIGS. MoS_2 doping is 10×10^{12} cm^{-2} and E_{CNL}= 0.2 eV. The contact geometries are (a) edge contact and (d) top contact. We indicate the experimental barrier height of previously investigated devices [4] using yellow shapes.

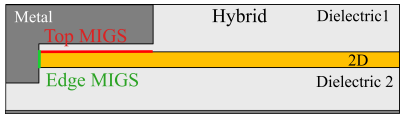

Fig. 6. Location of MIGS in a hybrid contact. Similar locations are used for edge and top contact.

Metal contact (Ti, Ni, Pt)	Edge	Top
D_{IT} (cm^{-2} eV^{-1})	~ 1.2×10^{14}	~ 1.3×10^{14}
E_{CNL}(eV)	0.2	0.2
MIGS (cm^{-2})	~ 2.4×10^{13}	~ 2.6×10^{13}
DFT MIGS (cm^{-2})	~ 2.3×10^{13}	~ 1.2×10^{13}

Table I. Contains the MIGS data of the different contact geometries

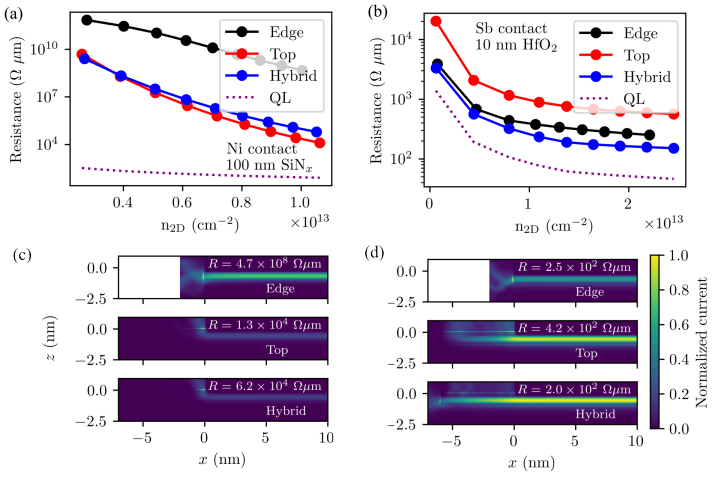

Fig. 7. Contact resistance vs. carrier concentration in an (a) Ni contact high barrier and pinning and (b) Sb contact for low barrier and pinning for different contact geometries. (c) and (d) show the corresponding current densities at the maximal carrier concentration according to (a) and (b).

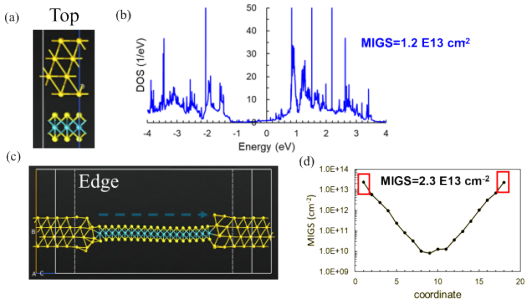

Fig. 8. (a) Structure of top contact in QuantumATK. (b) Density of states of the MoS_2 monolayer as function of energy. (c) Structure of edge contact in QuantumATK. (d) MIGS density as a function of x-coordinate.

Potentials:

$$\nabla\cdot(\bar{\epsilon}(x,z)\nabla V(x,z)) = e\left[N_D(x,z)+Q_{IT}(x,z)-n(x,z)\right] \quad (1)$$

$$n(x,z) = N\frac{m^* k_B T}{\pi\hbar^2 t_{2D}}\ln\left[1+\exp\left(\frac{E_F - eV(x,z)}{k_B T}\right)\right] \quad (2)$$

$$U_{IFBL}(r,\theta;\Omega) = \frac{-e^2}{8\pi\epsilon r}\int_0^\infty d\alpha \frac{\sinh(\alpha\pi)\cosh(2\alpha\theta)-\sinh(\alpha(\pi-\Omega))}{\sinh(\alpha\Omega)\cosh(\alpha\pi)} \quad (3)$$

MIGS:

$$\text{MIGS} = Q_{IT} = D_{IT}\cdot(E_F - E_{CNL}) \quad (4)$$

$$\text{SBH} = S\,(\text{WF} - \text{EA}) + (1-S)\,(E_C - E_{CNL}) \quad (5)$$

Transport:

$$H = -\frac{\hbar^2}{2}\nabla\cdot\left(\frac{1}{m^*(x,z)}\nabla\right) + \frac{\hbar^2 k_y^2}{2m^*(x,z)} + U(x,z) \quad (6)$$

$$[EI - H - \Sigma]\psi = B \quad (7)$$

$$T = 1 - \frac{|B_{out}^{-1}\psi_{out}|^2 v_{out}}{v_{in}} \quad (8)$$

$$\frac{1}{\rho_c} = \frac{2e^2}{h}N\int_{-\infty}^{\infty} dE\left|\frac{df(E)}{dE}\right|\int_{-\infty}^{\infty}\frac{dk_y}{2\pi}T(k_y,E) \quad (9)$$